Fusion of Low-Density LiDAR Data with RGB Images for Plant 3D Modeling

Manuel F. Garcia, Diego Mendez*, Julian D. Colorado
Department of Electronics Engineering, Pontificia Universidad Javeriana, Bogotá, Colombia.
*Corresponding author: diego-mendez@javeriana.edu.co

***Abstract*—Plant architecture is defined as the three-dimensional modeling of the plant's morphology for extracting relevant phenological traits. Most applications rely on expensive high-density LiDAR devices for enabling high-throughput mapping. In this paper, we explore the use of low-cost LiDAR equipment by using a sensor fusion approach. The proposed method is based on the fusion of LiDAR-acquired low resolution 3D point cloud data with high resolution 2D imagery. We use an extrinsic calibration method that requires oversampling to enhance the data fusion from both sensors. As a result, we increased the resolution of the output 3D model of the plant.**

***Index Terms*—plant architecture, LiDAR, sensor fusion, RGB imagery, plant phenotyping.**

I. Introduction

Plant phenotyping requires the use of high resolution sensors to characterize specific traits for plant breeding or the remote monitoring of the crop [7]. In this regard, defining three-dimensional (3D) models for plant morphology has recently enabled new approaches for understanding how genome features are associated with plant traits, e.g, leaf area and angle for chlorophyll absorption and nitrogen status, plant height for biomass production, among other geometrical variables [8], [3].

Most works rely on high-density LiDAR devices, stereoscopic camera arrays [12], [4], [21] or time-of-flight cameras [22], [5], [26], [9], [23] in order to capture 3D plant data [25]. Although these sensors enable high resolution 3D models of the plant structure, the high costs and size of these sensors limit in-field sensing. Here, we propose the use of low-cost small sensors that can operate directly in the field. Our goal is to explore simple sensor fusion algorithms that allow for real-time plant 3D modeling. Given that, we propose the use of a low-density Light Detection and Ranging (LiDAR) device and a high-resolution multispectral camera for acquiring 3D point cloud data of the plants that are combined with RGB/NIR pixels from the 2D imagery. A data fusion approach is applied for the 3D reconstruction, allowing for a non-destructive phenotyping system.

An important body of work from the specialized literature reports the use of digital plant models for the extraction of vegetation indices [24], [14], [10], which enable the characterization of sunlight absorption by calculating plant reflectances at different wavelengths [19], [2], [6]. In [1] and [13], a 4D plant modeling approach is proposed, where the 3D morphological data is mapped with each spectral band independently, with the aim of re-constructing the spatial information of the vegetation indices based on the geometry of the plant [17].

In order to generate a comprehensive digital model from the data fusion between 2D images and 3D data, several algorithms have been proposed, such as: perspective projections [11], Gaussian regressions [20], mutual information [18], and sensor extrinsic calibration methods [15], [16]. Here, we apply an extrinsic calibration method to determine a projection matrix that allows for the alignment between the 3D points generated by the LiDAR and the pixels generated by the RGB camera. Subsequently, an interpolation algorithm is applied for the data fusion.

The rest of the document is organized as follows: Section II details on the proposed mechanism for calibration and interpolation, Section III shows the experimental results and the corresponding analysis, and finally, Section IV concludes the paper and presents our future work.

II. Proposed Mechanisms and Setup

An architectural representation of our proposal is shown in Figure 1. In our approach to implement a fusion between LiDAR data and RGB images, an extrinsic calibration method is required, which is composed by three main components: (i) The usage of a diamond-shaped calibration board and finding the board's vertices (key-points) in the image generated by the camera and in the point cloud generated by the LiDAR. (ii) The implementation of a Random Sample Consensus (RANSAC) algorithm to find a plane that fits the sensed 3D points and projects them into the found plane. (iii) The application of a least squares regression method for finding the projection matrix that allows the alignment of the sensor's data.

The implemented calibration pattern consists in a diamond shaped cardboard with one black half and another white half, as it can be seen in Figure 2. Subsequently, in order to find the key-points of the calibration pattern in the 2D image, a Harris corner detector is used.

In order to select the 3D key-points, a plane P that satisfies as many 3D points as possible using the RANSAC algorithm must be estimated. Once the plane P is obtained, the 3D points have to be projected onto the plane. This additional step is required since non-uniform depth measurements are being obtained on this flat object, due to the low precision of the used LiDAR. As seen in Figure 3, by finding the plane that passes through the greatest number of points and projecting them onto that plane, we reduce the deviation due to the sensor's error.

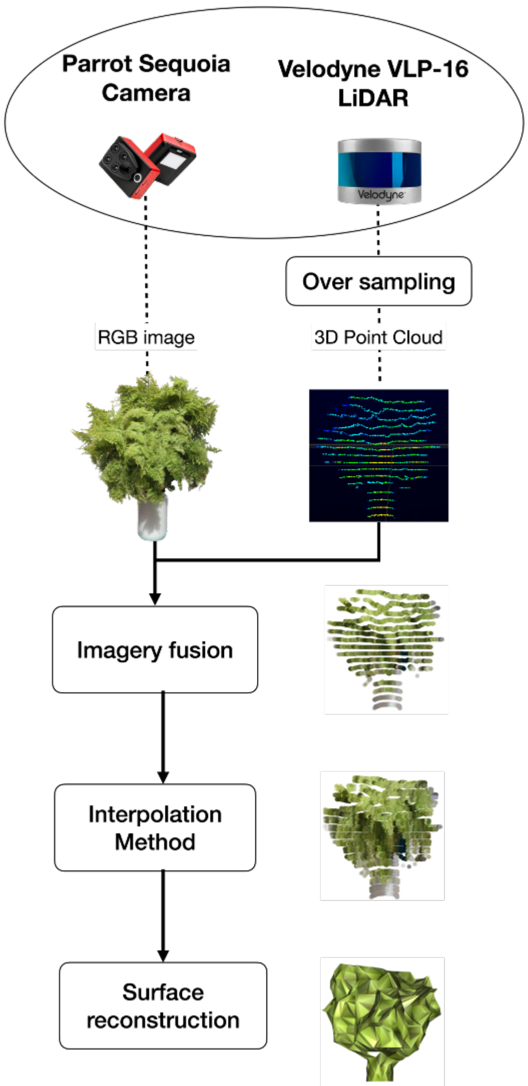

Figure 1: General diagram of the proposed fusion mechanism.

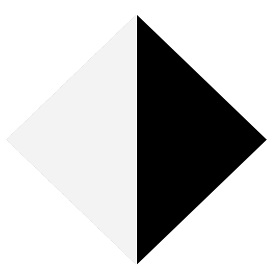

Figure 2: Diamond shaped calibration pattern.

Once the plane that passes through the majority of 3D points has been found, the point cloud is filtered only leaving the points that are at the ends of each laser in the LiDAR, which belong to the edge of the calibration pattern. Now, having those edge points and using the RANSAC algorithm again but only including the (x, z) coordinates of the points, a line that passes through the greatest number of points for each edge of the data is found, and with the intersection of the lines the (x, z) coordinates of the key-points are found (see Figure 4). Finally, those key-points are projected on the P plane for estimating

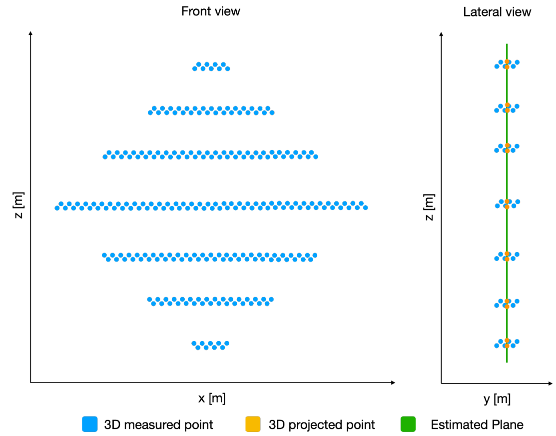

Figure 3: Measured vs projected points on plane P for the calibration pattern.

the values of their y-axes, thus obtaining the key points.

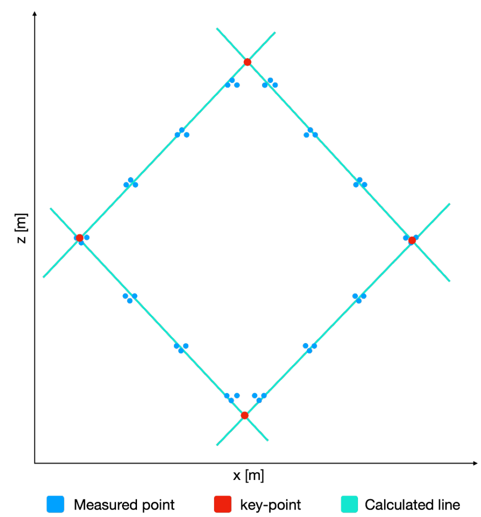

Figure 4: Edge estimation for key-point detection.

The method for aligning a 3D LiDAR point with its correspondent image pixel consists of using a least-squares regression for calculating the projection matrix, which is formulated as follows:

$$\begin{pmatrix} u \\ v \\ 1 \end{pmatrix} = \begin{pmatrix} f_u & 0 & u_0 \\ 0 & f_v & v_0 \\ 0 & 0 & 1 \end{pmatrix} \begin{pmatrix} R & t \\ 0 & 1 \end{pmatrix} \begin{pmatrix} z \\ y \\ z \\ 1 \end{pmatrix}$$

$$\begin{pmatrix} u \\ v \\ 1 \end{pmatrix} = C \begin{pmatrix} z \\ y \\ z \\ 1 \end{pmatrix}$$

$$\begin{pmatrix} u \\ v \\ 1 \end{pmatrix} = \begin{pmatrix} m_{11} & m_{12} & m_{13} & m_{14} \\ m_{21} & m_{22} & m_{23} & m_{24} \\ m_{31} & m_{32} & m_{33} & m_{34} \end{pmatrix} \begin{pmatrix} z \\ y \\ z \\ 1 \end{pmatrix}$$

where f_u and f_v are the effective focal lengths, (u_0, v_0) is the center point of the image plane, and R and t are the rotation and the translation matrices.

In this project we are utilizing the 16-channel Velodyne VLP-16 LiDAR, which generates data with very low vertical resolution, with big areas that have no mapped points, as seen in Figure 3. For this reason, it is necessary to use an interpolation algorithm estimate the missing points in these areas.

Algorithm 1: Interpolation Algorithm

x-axis: horizontal axis.
z-axis: vertical axis.
y-axis: depth axis.
input : A Point Cloud Data pcd of size $m \times 4$
input : A RGB image img
output: A denser Point Cloud Data of size $m \times 4$
Sort pcd by channels;
Sort pcd from lowest to highest X value;
$prPoint \leftarrow None$;
$channels \leftarrow 16$;
$interpPcd \leftarrow []$;
$YThreshold \leftarrow$ threshold for maximum Y distance between interpolated point and its adjacent points;
for $i \leftarrow 1$ **to** $chanels$ **do**
  $aChannel \leftarrow channels - i$;
  $aPcd \leftarrow$ filter pcd by $aChannel$;
  $nChannel \leftarrow channels - 1 - i$;
  $nPcd \leftarrow$ filter pcd by $nChannel$;
  $lenAPcd \leftarrow$ len of $aPcd$;
  for $r \leftarrow 0$ **to** $lenAPcd$ **do**
    if *($prPoint$ is $None$)* **then**
      $prPoint \leftarrow$3D point of $aPcd$ in r row ;
    else
      $aPoint \leftarrow aPcd[r]$;
      $val2f \leftarrow \frac{aPoint['X'] + prPoint['X']}{2}$;
      $nCPoint \leftarrow$close 3D point to $val2f$ in $nPcd$;
      $iPPoint \leftarrow$ center of gravity value of the triangle formed by the (X, Z) values of $prPoint$, $aPoint$, $nCPoint$, Figure 5 ;
      $plane \leftarrow$ plane that fit in $prPoint$, $aPoint$, $nCPoint$, Figure 6;
      $iPPoint['Y'] \leftarrow$ projected Y value of $iPPoint$ in $plane$;
      $HSVColorIpP \leftarrow$ get the HSV color that $iPPoint$ point has in the img image;
      if *($HSVColorIpP$ is in color segmentation defined by the color of $prPoint$, $aPoint$, $nCPoint$)* **then**
        $YMean \leftarrow$ mean Y value between $prPoint$, $aPoint$, $nCPoint$;
        $diff \leftarrow 100 - \frac{iPPoint['Y'] \times 100}{YMean}|$;
        if *($diff \leq YThreshold$)* **then**
          $interpPcd \leftarrow$append $iPPoint$ to $interpPcd$;
        else
      else
      end
    end
  end
end
$pcd \leftarrow$append $interpPcd$ to pcd;

For this purpose, we select three different 3D points to form a triangle and estimate the plane that passes through these three points (see Figure 5). Then, the center of the triangle is calculated and projected on the plane to obtain its depth (see Figure 6). To determine if this new estimated point is valid, thresholds are used in the estimated depth and the color corresponding to that point in the RGB image. The pseudocode of this interpolation is presented in Algorithm 1.

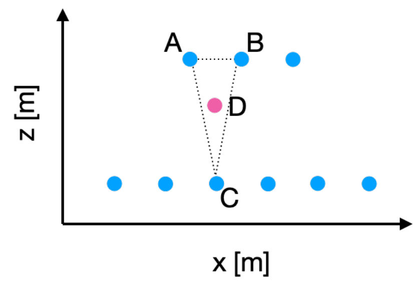

Figure 5: Center of gravity of the triangle formed between the points A, B, C.

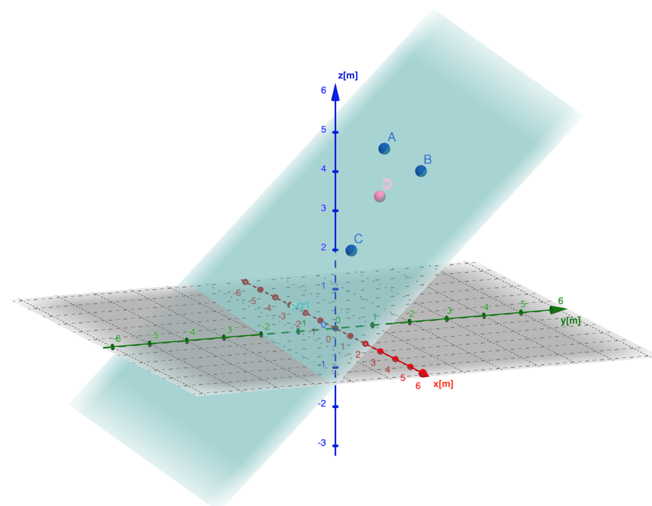

Figure 6: Projection of the gravity center point onto the plane.

III. Experimental Results and Analysis

This section provides a detailed description of how the experiments were carried out and the results obtained. We will present the details on the imagery fusion scheme, the process and results of implementing the interpolation algorithm, and finally, a surface reconstruction comparison using a point cloud with or without interpolation.

A. Imagery Fusion

For the extrinsic calibration of the LiDAR with the camera for achieving the imagery fusion, the diamond shaped calibration pattern (see Figure 2) was used, taking RGB images and point clouds of the calibration board for different distances and angles. Then, using the Harris corner detector, the key points were found on each of the 2D images, as seen in Figure 7.

To find these key-points in a 3D space, the point cloud was filtered so that only the points belonging to the board remained. Then, by applying the aforementioned technique to detect the vertices of the calibration pattern, the 3D key points were extracted (see Figure 8). Since the calibration matrix that we want to obtain through the least square regression has 12 unknowns, it is important to highlight that at least 12 key-points are required.

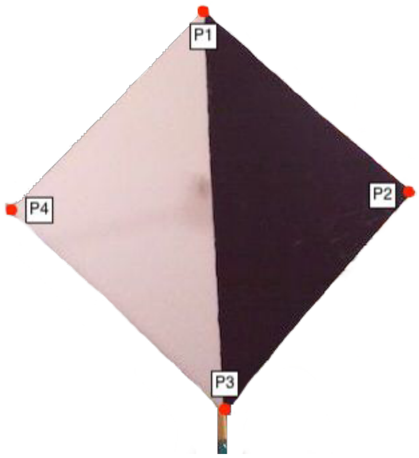

Figure 7: Key-points detection in the RGB image of the calibration pattern.

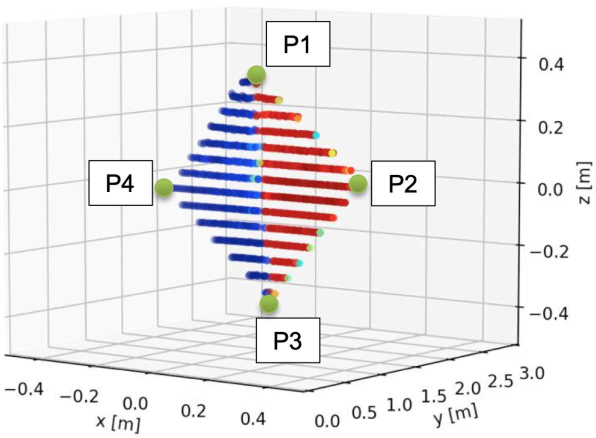

Figure 8: Key-points $(P1, P2, P3, P4)$ mapped in a 3D point cloud.

The result of the calibration can be seen in Figure 9, where each 3D point was mapped to a pixel of the 2D image, thus giving color to the point cloud according to the 2D image.

B. Interpolation and Oversampling

As it is shown in Figure 10, a fern was used as a test object to carry out the tests. This plant has an irregular surface and shape which makes it ideal for assessing the performance of the surface reconstruction algorithm to generate its shape.

The point cloud obtained by sensing the test object can be seen in Figure 11a. The undetected areas are due to the LiDAR low vertical resolution. By means of oversampling and applying the interpolation algorithm to the point cloud, a denser point cloud can be acquired. Because of the interpolation algorithm, the point cloud now integrates more information, filling the gaps of the sensor's dead zones (see Figure 11a).

C. Surface Reconstruction

To qualitatively analyse how the surface reconstruction is affected by the areas without LiDAR detection, a surface reconstruction mechanism was implemented on the point cloud

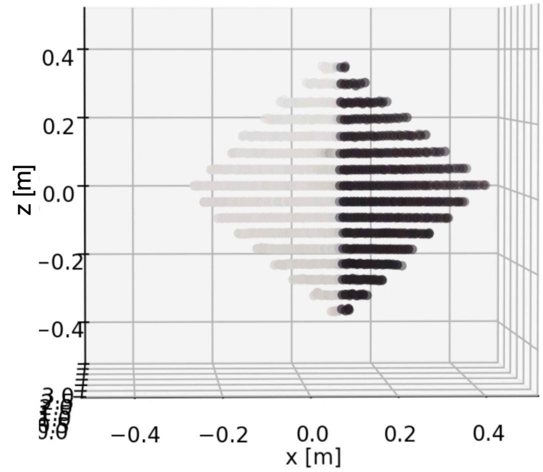

Figure 9: Cloud point colored as result of the calibration process.

Figure 10: A fern, the test object for these experiments.

without interpolation, with interpolation, and with interpolation and oversampling, varying the alpha parameter in each test (see Figure 11b). The alpha parameter indicates the distance between each 3D point to triangulate the mesh generation.

As seen in Figure 11b, due to the low vertical resolution of the LiDAR, there are areas of the object that were not reconstructed, even when varying the alpha parameter. By applying the surface reconstruction algorithm to the oversampled interpolated point cloud, those areas that previously could not be reconstructed can now be successfully generated.

IV. Conclusions and Future Work

The combination of data oversampling with the proposed interpolation method improved the resultant 3D model based on the data fusion between low-density LiDAR data points with high-resolution 2D imagery, as demonstrated in the results reported in Figure 11. The accuracy of the computed 3D models seems to properly match the geometrical properties of the testbed plant, as depicted in both plots (a) and (b) from Figure 11. Upcoming work is oriented towards the definition of a ground-truth model for the testbed, that enables the evaluation of performance metrics for the reconstructed 3D model. In addition, other spectral bands of the multispectral

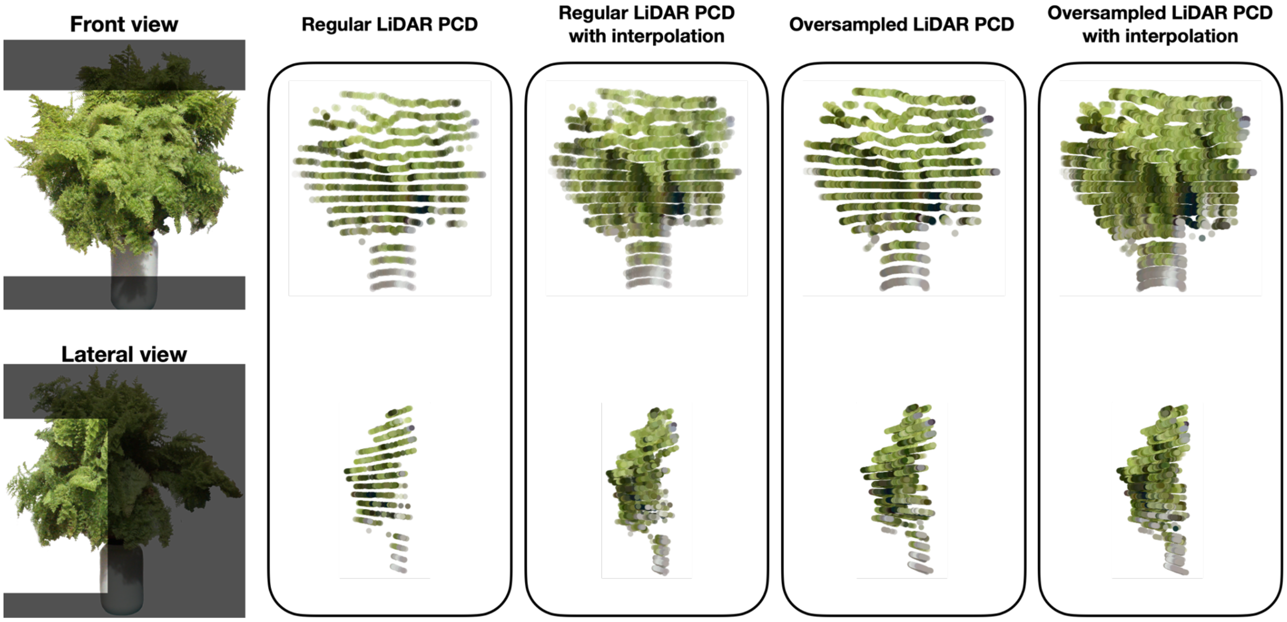

(a) Point cloud data comparison.

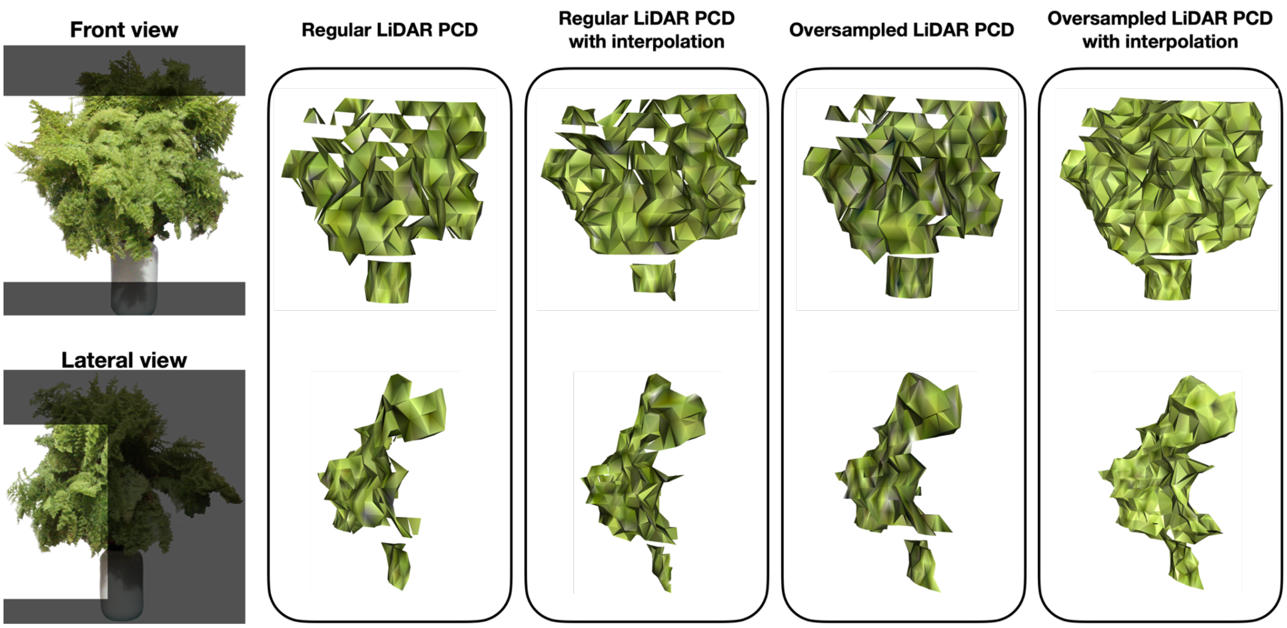

(b) Surface reconstruction comparison.

Figure 11: Comparison of result of the interpolation method for the point cloud data and the surface reconstruction.

camera will be considered within the data fusion process, with the aim of calculating volumetric vegetation indices that indicate the plant health status.

Acknowledgment

This work was funded by the OMICAS program: *Optimización Multiescala In-silico de Cultivos Agrícolas Sostenibles (Infraestructura y validación en Arroz y Caña de Azúcar)*, anchored at the Pontificia Universidad Javeriana in Cali and funded within the Colombian Scientific Ecosystem by The World Bank, the Colombian Ministry of Science, Technology and Innovation, the Colombian Ministry of Education and the Colombian Ministry of Industry and Turism, and ICETEX under GRANT ID: FP44842-217-2018.

References

[1] Federico Apelt, David Breuer, Zoran Nikoloski, Mark Stitt, and Friedrich Kragler. Phytotyping4D: A light-field imaging system for non-invasive and accurate monitoring of spatio-temporal plant growth. *Plant Journal*, 82(4):693–706, 2015.

[2] A. Bannari, D. Morin, F. Bonn, and A. R. Huete. A review of vegetation indices. *Remote Sensing Reviews*, 13(1-2):95–120, 1995.

[3] Nicolas Brichet, Christian Fournier, Olivier Turc, Olivier Strauss, Simon Artzet, Christophe Pradal, Claude Welcker, François Tardieu, and Llorenç Cabrera-Bosquet. A robot-assisted imaging pipeline for tracking the growths of maize ear and silks in a high-throughput phenotyping platform. *Plant Methods*, 13(1):1–12, 2017.

[4] Alexandra J. Burgess, Renata Retkute, Michael P. Pound, Sean Mayes, and Erik H. Murchie. Image-based 3D canopy reconstruction to determine potential productivity in complex multi-species crop systems. *Annals of botany*, 119(4):517–532, 2017.

[5] Supawadee Chaivivatrakul, Lie Tang, Matthew N. Dailey, and Akash D. Nakarmi. Automatic morphological trait characterization for corn plants via 3D holographic reconstruction. *Computers and Electronics in Agriculture*, 109:109–123, 2014.

[6] Martin Ecarnot, Frédéric Compan, and Pierre Roumet. Assessing leaf nitrogen content and leaf mass per unit area of wheat in the field throughout plant cycle with a portable spectrometer. *Field Crops Research*, 140:44–50, 2013.

[7] Noah Fahlgren, Malia A. Gehan, and Ivan Baxter. Lights, camera, action: High-throughput plant phenotyping is ready for a close-up. *Current Opinion in Plant Biology*, 24:93–99, 2015.

[8] Robert T. Furbank and Mark Tester. Phenomics - technologies to relieve the phenotyping bottleneck. *Trends in Plant Science*, 16(12):635–644, 2011.

[9] Haiou Guan, Meng Liu, Xiaodan Ma, and Song Yu. Three-dimensional reconstruction of soybean canopies using multisource imaging for phenotyping analysis. *Remote Sensing*, 10(8), 2018.

[10] Li He, Xiao Song, Wei Feng, Bin Bin Guo, Yuan Shuai Zhang, Yong Hua Wang, Chen Yang Wang, and Tian Cai Guo. Improved remote sensing of leaf nitrogen concentration in winter wheat using multi-angular hyperspectral data. *Remote Sensing of Environment*, 174:122–133, 2016.

[11] Fumiki Hosoi, Sho Umeyama, and Kuangting Kuo. Estimating 3D chlorophyll content distribution of trees using an image fusion method between 2D camera and 3D portable scanning lidar. *Remote Sensing*, 11(18), 2019.

[12] Fang Hui, Jinyu Zhu, Pengcheng Hu, Lei Meng, Binglin Zhu, Yan Guo, Baoguo Li, and Yuntao Ma. Image-based dynamic quantification and high-accuracy 3D evaluation of canopy structure of plant populations. *Annals of Botany*, 121(5):1079–1088, 2018.

[13] Kenta Itakura, Itchoku Kamakura, and Fumiki Hosoi. Three-dimensional monitoring of plant structural parameters and chlorophyll distribution. *Sensors (Switzerland)*, 19(2), 2019.

[14] Fei Li, Bodo Mistele, Yuncai Hu, Xinping Chen, and Urs Schmidhalter. Reflectance estimation of canopy nitrogen content in winter wheat using optimised hyperspectral spectral indices and partial least squares regression. *European Journal of Agronomy*, 52:198–209, 2014.

[15] Juan Li. *Fusion of lidar 3d points cloud with 2d digital camera image*. Master of science in electrical and computer engineering, Oakland University Rochester, Michigan, 2015.

[16] Juan Li, Xiang He, and Jia Li. 2D LiDAR and camera fusion in 3D modeling of indoor environment. *Proceedings of the IEEE National Aerospace Electronics Conference, NAECON*, 2016-March:379–383, 2016.

[17] Ren C. Luo, Chih Chen Yih, and Kuo Lan Su. Multisensor fusion and integration: Approaches, applications, and future research directions. *IEEE Sensors Journal*, 2(2):107–119, 2002.

[18] Andrew Mastin, Jeremy Kepner, and John Fisher. Automatic registration of LIDAR and optical images of urban scenes. *2009 IEEE Computer Society Conference on Computer Vision and Pattern Recognition Workshops, CVPR Workshops 2009*, 2009 IEEE:2639–2646, 2009.

[19] P. B. Reich, D. S. Ellsworth, and M. B. Walters. Leaf structure (specific leaf area) modulates photosynthesis-nitrogen relations: Evidence from within and across species and functional groups. *Functional Ecology*, 12(6):948–958, 1998.

[20] Varuna De Silva, Jamie Roche, and Ahmet Kondoz. Robust Fusion of LiDAR and Wide-Angle Camera. 2018.

[21] H. Sinoquet, S. Thanisawanyangkura, H. Mabrouk, and P. Kasemsap. Characterization of the light environment in canopies using 3D digitising and image processing. *Annals of Botany*, 82(2):203–212, 1998.

[22] Wei Su, Dehai Zhu, Jianxi Huang, and Hao Guo. Estimation of the vertical leaf area profile of corn (Zea mays) plants using terrestrial laser scanning (TLS). *Computers and Electronics in Agriculture*, 150(17):5–13, 2018.

[23] Suresh Thapa, Feiyu Zhu, Harkamal Walia, Hongfeng Yu, and Yufeng Ge. A novel LiDAR-Based instrument for high-throughput, 3D measurement of morphological traits in maize and sorghum. *Sensors (Switzerland)*, 18(4), 2018.

[24] Y. C. Tian, X. Yao, J. Yang, W. X. Cao, D. B. Hannaway, and Y. Zhu. Assessing newly developed and published vegetation indices for estimating rice leaf nitrogen concentration with ground- and space-based hyperspectral reflectance. *Field Crops Research*, 120(2):299–310, 2011.

[25] Manuel Vázquez-Arellano, Hans W. Griepentrog, David Reiser, and Dimitris S. Paraforos. 3-D Imaging Systems for Agricultural Application - A Review. *Sensors (Switzerland)*, 16(5), 2016.

[26] Manuel Vázquez-Arellano, David Reiser, Dimitrios S. Paraforos, Miguel Garrido-Izard, and Hans W. Griepentrog. Leaf area estimation of reconstructed maize plants using a time-of-flight camera based on different scan directions. *Robotics*, 7(4), 2018.